Growth of Giant Rodlike Micelles of Ionic Surfactant in the Presence of Al^{3+} Counterions

R. G. Alargova,[†] K. D. Danov,[†] P. A. Kralchevsky,*[,†] G. Broze,[‡] and A. Mehreteab[§]

Laboratory of Thermodynamics and Physico-chemical Hydrodynamics, Faculty of Chemistry, University of Sofia, 1126 Sofia, Bulgaria, Colgate-Palmolive Research and Development, Inc., Avenue Du Parc Industriel, B-4041 Milmort (Herstal), Belgium, and Colgate-Palmolive Co., Technology Center, 909 River Road, Piscataway, New Jersey 08854-5596

Received June 26, 1997. In Final Form: April 17, 1998

To interpret quantitatively experimental data for the growth of rodlike anionic surfactant micelles in the presence of Al^{3+} ions, we undertook experimental and theoretical investigations. We determined the micelle size, shape, and interactions by light scattering and examined the binding of Al^{3+} ions to the micelles by ultrafiltration. Independent static and dynamic light scattering measurements indicated that the effect of the micelle−micelle interactions in these solutions can be neglected. The major factor promoting the micelle growth turns out to be the binding of Al^{3+} ions to the micelle surfaces, which considerably affects the standard chemical potential of the aggregated surfactant molecules and can alter the micellization constant by orders of magnitude. The latter effect was described theoretically. The model of micelle growth, extended in this way, compared well with the experimental data. The model provides a quantitative description of the micelle size and charge as functions of the surfactant and electrolyte concentrations. It turns out that the rodlike micelles have a lower surface charge than the spherical ones, and this makes their growth energetically favorable. A practical application may follow from the markedly greater solubilization efficiency of the studied rodlike micelles compared to the spherical ones.

1. Introduction

As it is known, the spherical surfactant micelles undergo a transition to larger rodlike aggregates with the increase of surfactant concentration.[1] It was established experimentally that the formation of rodlike micelles of ionic surfactants is enhanced by the addition of electrolyte and/or decreasing the temperature,[2−10] as well as by increasing the length of the surfactant hydrocarbon chain.[11−13] Note that the aforementioned experimental studies were performed using *monovalent* (1:1) electrolyte.

It was recently established[14] that the presence of multivalent counterions (Ca^{2+}, Al^{3+}) in solutions of anionic surfactant (sodium dodecyl dioxyethylene sulfate, SDP2S) strongly enhances the formation of rodlike micelles. A qualitative explanation of this fact is that a multivalent counterion, for example, Al^{3+}, can bind together three surfactant headgroups at the micelle surface, thus causing a decrease of the area per headgroup.[14] In accordance with the theory by Israelachvili et al.,[1,15] this will induce a transition from spherical to cylindrical micelles.

The experiment[14] showed that the formation of rodlike micelles in the presence of multivalent counterions differs from the micellization in the presence of 1:1 electrolyte in several aspects:

(i) The multivalent counterions are much more effective than the monovalent counterions as promoters of the formation of rodlike micelles. For example, at 8 mM surfactant (SDP2S) concentration, the molar concentration of Na^+ needed to cause a transition from spherical to rodlike micelles is 230 times larger than the respective molar concentration of Al^{3+}.

(ii) In the presence of multivalent counterions, cylindrical micelles (of aggregation number up to 4000) appear at relatively low surfactant concentration[14] (from 2 to 8 mM) corresponding to *isotropic* solutions. In other words, the average distance between the micelles is larger than the micelle average length, and liquid−crystal-like ordering of micelles does not appear.

(iii) When the concentration of multivalent counterions is fixed and the surfactant concentration is varied, one observes cylindrical micelles at the *lower* surfactant concentrations and spherical micelles at the *higher* surfactant concentrations. This is exactly opposite the case of monovalent counterions. The explanation is that the transition from sphere to rod occurs at a given ratio of surfactant to electrolyte; in the excess of electrolyte (of

* To whom correspondence should be addressed. E-mail: Peter.Kralchevsky@LTPH.BOL.BG.
[†] University of Sofia.
[‡] Colgate-Palmolive Research and Development, Inc.
[§] Colgate-Palmolive Co., Technology Center.

(1) Israelachvili, J. N. *Intermolecular and Surface Forces*; Academic Press: London, 1991; Chapter 17.
(2) Mazer, N. A.; Benedek, G. B.; Carey, M. C. *J. Phys. Chem.* **1976**, *80*, 1075.
(3) Missel, P. J.; Mazer, N. A.; Benedek, G. B.; Young, C. Y.; Carey, M. C. *J. Phys. Chem.* **1980**, *84*, 1044.
(4) Hayashi, S.; Ikeda, S. *J. Phys. Chem.* **1980**, *84*, 744.
(5) Porte, G.; Appell, J.; Poggi, Y. *J. Phys. Chem.* **1980**, *84*, 3105.
(6) Porte, G.; Appell, J. *J. Phys. Chem.* **1981**, *85*, 2511.
(7) Hoffmann, H.; Klaus, J.; Thurn, H.; Ibel, K. *Ber. Bunsen-Ges. Phys. Chem.* **1983**, *87*, 1120.
(8) Chen, J.-M.; Su, T. M.; Mou, C. Y. *J. Phys. Chem.* **1986**, *90*, 2418.
(9) Missel, P. J.; Mazer, N. A.; Carey, M. C.; Benedek, G. B. *J. Phys. Chem.* **1989**, *93*, 8354.
(10) Lin, T.-L.; Tseng, M.-Y.; Chen, S.-H.; Roberts, M. F. *J. Phys. Chem.* **1990**, *94*, 7239.
(11) Tausk, R.; Overbeek, J. Th. G. *Colloid Interface Sci.* **1976**, *2*, 379.
(12) Nicoli, D. F.; Dawson, D. R.; Offen, J. W. *Chem. Phys. Lett.* **1979**, *66*, 291.
(13) Missel, P. J.; Mazer, N. A.; Benedek, G. B.; Carey, C. *J. Phys. Chem.* **1983**, *87*, 1264.
(14) Alargova, R.; Petkov, J.; Petsev, D.; Ivanov, I. B.; Broze, G.; Mehreteab, A. *Langmuir* **1995**, *11*, 1530.
(15) Israelachvili, J. N.; Mitchell, D. J.; Ninham, B. W. *J. Chem. Soc. Faraday Trans. 2* **1976**, *72*, 1525.

S0743-7463(97)00684-7 CCC: $15.00
Published on Web 06/30/1998

multivalent counterions), cylindrical micelles are formed, whereas in the excess of surfactant, the micelles are spherical.

It should also be noted that the giant cylindrical micelles in the presence of Al^{3+} studied in ref 14 are rather rigid: the persistent length of the thermally excited undulations is typically larger than the length of a micelle. Hence, in this case, one deals with *rod*like (rather than *worm*like) micelles.

The data for the micelle growth in the presence of 3:1 electrolyte reported in ref 14 do not conform (and should not be expected to conform) to the available theoretical models designed for the case of 1:1 electrolyte[3,15,16] (see the discussion in section 2.3 below). The latter fact stimulated us to undertake a theoretical study of the micellar growth in the presence of *multivalent* electrolyte. Moreover, we carried out some additional experiments in order to compare the data with the theoretical predictions.

As a basis of the theoretical interpretation below, we used the model by Missel et al.[3] (the "ladder model") which was recently extended to mixed micelles[17] and modified to account for the temperature effects with nonionics.[18] This theoretical model has been confirmed by several experimental works.[8−10,13] Its basic equations are summarized below for the needs of subsequent citation. Missel et al.[3] demonstrated that the expressions for the solute chemical potentials in an *ideal* solution

$$\mu_1 = \mu_1^0 + kT \ln X_1, \quad \mu_n = \mu_n^0 + kT \ln X_n \quad (1.1)$$

can be successfully applied to the micellar solutions of ionic surfactants at relatively high concentrations of 1:1 electrolyte; here X_1 and X_n are the mole fractions of the free monomers and the micelles of aggregation number n in the solution; μ_1^0 and μ_n^0 are the respective standard chemical potentials, k is the Boltzmann constant, and T is temperature. Then, the condition of chemical equilibrium, $\mu_n = n\mu_1$, is used to derive the micelle size distribution

$$X_n = X_1^n \exp[-(\mu_n^0 - n\mu_1^0)/kT] \quad (1.2)$$

As known from the experiment, the micelles of aggregation number $1 < n < n_0$ are unstable, and the more stable micelles have aggregation number $n \geq n_0$. Then, the mole fraction of surfactant monomers initially placed in the solution is

$$X = X_1 + \sum_{n=n_0}^{\infty} nX_n \quad (1.3)$$

Missel et al.[3] supposed that the micelles of aggregation number $n = n_0$ are spherical and that the bigger micelles have prolate sphero-cylindrical shape, see Figure 1. In other words, each micelle consists of a cylindrical part containing $n - n_0$ molecules and two hemispherical end caps, each of which contains $n_0/2$ molecules (Figure 1). Correspondingly, the standard chemical potential of a micelle is presented in the form

$$\mu_n^0 = \mu_{n_0}^0 + (n - n_0)\mu^0 \quad (1.4)$$

where $\mu_{n_0}^0$ is the standard chemical potential of a (spherical) micelle of aggregation number n_0 and μ^0 is the standard

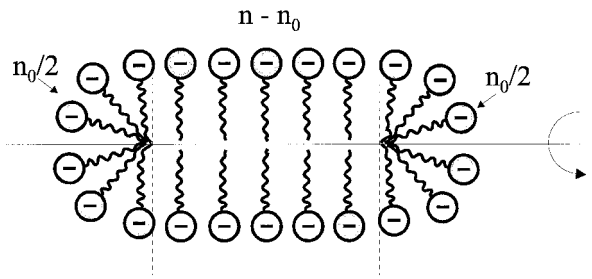

Figure 1. A schematic picture of a rodlike micelle.

chemical potential of each of the monomers in the cylindrical region. Combining eqs 1.2 and 1.4, one arrives at the distribution[3]

$$X_n = \frac{1}{K}\left(\frac{X_1}{X_B}\right)^n, \quad n \geq n_0 \quad (1.5)$$

where

$$K \equiv \exp[n_0(\mu_{n_0}^0/n_0 - \mu^0)/kT], \quad X_B = \exp[(\mu^0 - \mu_1^0)/kT] \quad (1.6)$$

Experimentally, the mass average aggregation number

$$\bar{n}_M \equiv \left(\sum_{n=n_0}^{\infty} n^2 X_n\right) / \sum_{n=n_0}^{\infty} nX_n \quad (1.7)$$

is measured by light scattering. From eqs 1.5−1.7 one can derive[3]

$$\bar{n}_M \approx n_0 + 2[K(X - X_1)]^{1/2} \quad (1.8)$$

In the original version of eq 1.8 (see ref 3) X_B is used instead of X_1; however, it was established[13] that $X_B \approx X_1$ with an accuracy about 5−15%. In our case $X_B \approx X_1$ is a good approximation, in so far as $X \gg X_B$, and the small differences between X_B and X_1 are immaterial for the precision of eq 1.8.

It was established[3] that eq 1.8 agrees well with the experimental data for SDS micelles in the presence of NaCl. On the other hand, as mentioned above, our experimental data for SDP2S in the presence of $AlCl_3$ + NaCl did not comply with eq 1.8 (see section 2.3 below). This could be attributed to the effect of the added 3:1 electrolyte on the electrostatic interactions in the system. One can distinguish the following two types of electrostatic effects in micellar solutions of ionic surfactants:

(i) Electrostatic *energy of micellization*. This is the work to bring a charged surfactant monomer from "infinity" and to incorporate it within a micelle with account for the electric double layer formed around the micelle.[9,19,20]

(ii) Electrostatic interaction *between the micelles* in solution. This effect can be important for higher micelle concentrations and/or lower electrolyte concentrations; it is investigated in refs 21−23.

Our analysis (see below) shows that, for the studied system effect, (ii) is negligible, whereas the effect (i) is of primary importance. In fact, when we tried to interpret the data for the growth of micelles in the presence of Al^{3+}

(16) Mukerjee, P. *J. Phys. Chem.* **1972**, *76*, 565.
(17) Thomas, H. G.; Lomakin, A.; Blankschtein, D.; Benedek, G. B. *Langmuir* **1997**, *13*, 209.
(18) Kato, T.; Kanada, M.; Seimiya, T. *J. Colloid Interface Sci.* **1996**, *181*, 149.
(19) Mitchell, D. J.; Ninham, B. W. *J. Phys. Chem.* **1983**, *87*, 2996.
(20) MacKintosh, F. C.; Safran, S. A.; Pincus, P. A. *Europhys. Lett.* **1990**, *12*, 697.
(21) Ben-Shaul, A.; Gelbart, W. M. *J. Phys. Chem.* **1982**, *86*, 316.
(22) Odijk, T. *J. Chem. Phys.* **1990**, *93*, 5172.
(23) Mileva, E. *J. Colloid Interface Sci.* **1996**, *178*, 10.

ions, our first hypothesis was that the differences between our data and the ladder model can be attributed to the electrostatic micelle−micelle interactions. The latter should be stronger than those in the system studied by Missel et al.[3] because of the lower ionic strength of our solutions. However, we noticed next that, in spite of the lower value of the ionic strength, it is large enough to make the electrostatic micelle−micelle interactions an effect of higher order. Indeed, in our case, the Debye screening length is $\kappa^{-1} \approx 2$ nm (see eq 3.13 below), whereas the average length of the rodlike micelles is on the order of dozens of nm. Hence, the electrostatic micelle−micelle interactions should be dominated by the steric (excluded volume) interactions, just as it is in the case of the micelles with Na^+ studied in ref 3.

We should mention in advance the following. After a closer inspection of the problem, we established that the key for understanding the micelle growth is the fact that the Al^{3+} ions do bind strongly to the anionic surfactant headgroups on the micelle surface. This effect can be detected by independent surface tension measurements, the results of which have been reported and interpreted in a separate paper.[24] Physically, the binding of Al^{3+} ions to the micelle surface considerably affects the standard chemical potential of the surfactant monomers incorporated within the micelles. The respective change in the difference, $\mu_{n_0}^0/n_0 - \mu^0$, enters eq 1.6 multiplied by the aggregation number $n_0 \approx 56$ in the argument of an exponential function. That is the reason why the binding of counterions quantitatively has a very strong effect on the value of the micellization constant, K (see eq 1.6), which can vary by orders of magnitude when the bulk concentration of Al^{3+} is varied (see also Figure 14 below). In other words, for the investigated micellar solutions the effect of micelle−micelle electrostatic and steric interactions on the micelle growth turns out to be quite immaterial when compared with the powerful effect of the counterion binding on the standard chemical potential of the aggregated monomers and, consequently, on the micellization constant, K.

In the next section, we present and discuss experimental data obtained by ultrafiltration and laser light scattering. Further, we propose a quantitative interpretation of the experimental findings. We pay special attention to the dependence of the equilibrium constant (the growth parameter), K, on the electrolyte concentration and to the binding of Al^{3+} ions to the micelles. The results reveal the cause for the micelle growth and give information about the surface charge of the micelles and its variation with the length of the rodlike aggregates.

2. Experiments and Discussion

2.1. Solutes and Solutions. The surfactant used in the present work was sodium dodecyl dioxyethylene sulfate (SDP2S), Empicol ESB70, Wilson Co. (UK), with the structure $CH_3(CH_2)_{11}(OC_2H_4)_2OSO_3Na$. The ionic strength of the added electrolyte was $I_0 = 0.024$ M in all experiments. It was adjusted with a mixture of NaCl and $AlCl_3 \cdot 6H_2O$ (Sigma). All micellar solutions were prepared by using deionized water (Milli-Q, Organex grade). All experiments with $AlCl_3$ were carried out between 18 and 24 h after the preparation of the solutions.

It might seem questionable whether the Al^{3+} ions exist in the solutions in trivalent form or in the form of complexes with the OH^- ions. It is known that, below pH = 4.0, the dissolved Al is present mostly in the form of trivalent ions.[25−27] In our case, the dissolved $AlCl_3$ decreases the pH of the solutions to about 3.0−3.5, and our estimates based on the data[26,27] about the stability of the various compounds, $Al(OH)^{2+}$, $Al(OH)_2^+$, and $Al(OH)_3$, showed that the fraction of Al^{3+} is above 98% at pH = 3.0 and above 95% at pH = 3.5.

The effect of pH on micellar size was checked using samples containing 8 mM SDP2S and 0.024 M NaCl at pH = 5.5. Then the pH was lowered by adding small portions of 0.1 M HCl at continuous stirring. The micelle hydrodynamic radius, R_H, was measured by light scattering (see section 2.2) for samples with pH = 2.5, 3.5, and 5.5; for each solution the values of R_H have been measured after 18, 24, and 48 h from the preparation of the solution. The measured values of R_H were found to be the same, $R_H = 2.2 \pm 0.3$ nm, for the studied ranges of pH and solution age. Therefore, one can conclude that micellar growth is not affected by the variation of pH in the range 2.5−5.5 when Al^{3+} ions are absent. In other words, the relatively low pH of the solutions containing $AlCl_3$ (pH = 3−3.5) is not the factor which causes the growth of the long rodlike micelles; it seems rather that the presence Al^{3+} ions promotes the micelle growth in these solutions.

We determined the critical micellization concentration (cmc) of SDP2S in the presence of Al^{3+} by measuring the average intensity of the scattered light (static light scattering, SLS) as a function of the surfactant concentration. The appearance of micelles led to a break point in the concentration dependence after which the intensity of the scattered light increased linearly with the micellar concentration. Results for the cmc of SDP2S in the presence of different amounts of monovalent (Na^+) and trivalent (Al^{3+}) counterions are presented and discussed in ref 24. It is necessary to mention only that the cmc depends mostly on the ionic strength, I_0, and rather weakly on the specific type of the dissolved ions, a fact which is consistent with the results of other studies.[28,29] For SDP2S we experimentally established[24] that ln cmc decreases linearly with ln I_0 in the concentration range $0.024 < I_0 < 0.128$ M

$$\ln \text{cmc} = -11.444 - 0.7573 \ln I_0 \qquad (2.1)$$

Similar dependence has been experimentally established for other surfactants.[30]

The determination of cmc by static light scattering was not very accurate in our case. The reason for this is that cmc is very low, and the presence of Al^{3+} ions causes precipitation of the surfactant in some solutions (typically for concentrations below cmc). To verify the SLS results, we obtained[24] independent data for cmc by measuring surface tension isotherms of SDP2S at $I_0 = 0.024$ M in the presence of NaCl or $AlCl_3$ only. In both cases we determined cmc $\approx 1 \times 10^{-4}$ M which is close to the result from the static light scattering.

In ref 14 we established experimentally that the transition from spherical to rodlike micelles is influenced by the surfactant-to-multivalent-counterion ratio defined as follows:

$$\xi = c_{SM}/(Zc_{AT}) \qquad (2.2)$$

where c_{SM} is the molar concentration of surfactant molecules in micellar form, c_{AT} is the total molar concentration of the multivalent counterion (of valence $Z > 1$) in solution. In other words, ξ equals the ratio of the net charge of the micellar ionizable groups to the net charge of the dissolved multivalent counterions (Al^{3+}, Ca^{2+}, etc.). One could expect that one Al^{3+} ion can bind three anionic surfactant headgroups at the micelle surface. This would lead to a decrease of the optimal area per headgroup and will favor the growth of the micelles, as predicted by the theoretical model of Israelachvili et al.[15] For $\xi < 1$ there is an excess of Al^{3+} ions in the solution and one experimentally establishes that long rodlike micelles grow in the solution.[14] On the other hand, for $\xi > 1$ the amount of the Al^{3+} ions in the

(24) Alargova, R. G.; Danov, K. D.; Petkov, J. T.; Kralchevsky, P. A.; Broze G.; Mehreteab, A. *Langmuir* **1997**, *13*, 5544.

(25) Marchenko, Z. *Photometric determination of the elements*; Mir: Moscow, 1971. (In Russian.)

(26) Lurie, Y. Y. *Handbook of Analytical Chemistry*; Khimia: Moscow, 1989. (In Russian.)

(27) Bontchev, P. *Introduction to Analytical Chemistry*; Nauka i Izkustvo: Sofia, 1985. (In Bulgarian.)

(28) Tanford, C. *The Hydrophobic Effect: Formation of Micelles and Biological Membranes*; Wiley: New York, 1980; Chapter 7.

(29) Oko, M. U.; Venable, R. L. *J. Colloid Interface Sci.* **1971**, *35*, 53.

(30) Hunter, R. J. *Foundations of Colloid Science*; Clarendon Press: Oxford, 1987.

solution is not sufficient to interconnect all of the anionic headgroups on the micelle surfaces. Experimentally, one finds that for $\xi > 1$, the surfactant is organized into small spherical micelles.[14]

The dependence of micelle size on the surfactant concentration was experimentally studied at constant ratio, ξ, and constant ionic strength, $I_0 = 0.024$ M, of the input electrolyte (NaCl and $AlCl_3$). To achieve an increase of ξ at fixed I_0, we added to the solution of the lowest ξ a portion of NaCl solution with the same ionic strength, $I_0 = 0.024$ M. Thus, the experimentally controlled variables are the surfactant concentration, c_s, the surfactant-to-aluminum ratio, ξ, and the ionic strength of the added electrolyte, I_0. It should be noted that I_0 is not the true ionic strength of the solution in so far as it does not include the contribution of the dissolved ionic surfactant, SDP2S. A more rigorous calculation of the true ionic strength, I_t, is given in section 3.2 below. We will mention in advance that, for our solutions, the value of I_t turns out to be very close to I_0.

As already noted, in the presence of Al^{3+}, the variation of ξ has a strong effect on the size of the micelles; for instance, a decrease of ξ from 1.2 to 0.67 leads to a 60-fold increase of the mean mass aggregation number of the micelles, $\bar{n}_M$. To obtain this information in ref 14 and in the present study, we used the dynamic and static light scattering techniques described below.

2.2. Light Scattering Experiments. The light scattering measurements were performed using the Autosizer 4700C (Malvern, Ins., U.K.) supplied with a K7032 CE 8-multibit correlator. The light source was an argon laser (Innova 70, coherent), operating at a 488 nm wavelength of vertical plane polarized light. The apparatus has the capability of working at different scattering angles in the range 10 to 150°. The temperature in all experiments was automatically maintained at 27 ± 0.1 °C. The samples were filtered with Millex (Millipore, Bedford, MA) filters 100, 220, and 450 nm before the measurements were taken to avoid the influence of dust particles. The surfactant concentration was varied from 0.075 to 0.3 wt % (2−8 mM) of SDP2S. This concentration range was low enough to avoid multiple light scattering. On the other hand, the concentration of the SDP2S micelles was high enough to allow measurements at low laser power (between 50 and 100 mW). Thus, the results were not influenced by a local heating of the samples caused by the beam. Measurements at various powers of the initial laser beam were carried out; the obtained results were not sensitive to the laser power in the framework of the experimental error, i.e., effects of local heating were not observed. In fact, the higher laser power (100 mW) was needed for solutions containing small micelles formed at low surfactant concentration, while the larger micelles at higher concentrations were observed by using the minimum laser power (close to 50 mW).

The autosizer 4700C works in homodyne mode of operation. Hence, the photomultiplier detected the light intensity autocorrelation function[31]

$$g^{(2)}(\tau) = \frac{\langle E_S^*(t)\, E_S(t)\, E_S^*(t+\tau)\, E(t+\tau)\rangle}{\langle I_S^2\rangle} \qquad (2.3)$$

where E_S is the intensity of the scattered electric field, I_S is the intensity of the scattered light, and $g^{(2)}(\tau)$ is related to the field autocorrelation function $g^{(1)}(\tau)$ as follows[31]

$$g^{(2)}(\tau) = 1 + |g^{(1)}(\tau)|^2, \quad g^{(1)}(\tau) = \frac{\langle E_S^*(t+\tau)\, E_S(\tau)\rangle}{\langle I_S\rangle} \qquad (2.4)$$

Further, $g^{(1)}(\tau)$ is expressed as a cumulant expansion

$$\ln(g^{(1)}(\tau)) = \sum_m K_m \frac{(-\tau)^m}{n!}, \quad K_m \equiv (-1)^m \lim_{\tau\to 0} \frac{\mathrm{d}^m}{\mathrm{d}\tau^m} \ln(g^{(1)}(\tau)) \qquad (2.5)$$

For system of non-interacting particles one can write[31]

$$K_1 = Dq^2, \quad K_2 = K_3 = \ldots = 0 \qquad (2.6)$$

where D is the Stokes−Einstein diffusion coefficient, $q = (4\pi n/\lambda)\sin(\theta/2)$ is the wavenumber, n is the refractive index of the solution, λ is the laser source wavelength, and θ is the scattering angle. Thus the *dynamic* light scattering technique gives the average diffusivity of the micelles, D, which is related to the micelle *hydrodynamic radius*, R_H, by means of the Stokes−Einstein formula $R_H = kT/(6\pi\eta D)$, see, e.g., refs 31 and 32. Of course, if the micelles are non-spherical, R_H is an apparent radius.

Equations 2.5−2.6 define the so-called "z-average" diffusion coefficient and describe the cumulant method (monomodal analyses). This method assumes nothing about the form of the size distribution and simply fits a polynomial to the logarithm of the normalized autocorrelation function. To determine the mass average diffusion coefficient of the micelles, we used the commercial Autosizer 4700 produced by Malvern Instruments Ltd. (UK). It is equipped with built-in software based on the exponential sampling method-multimodal analyses, especially designed for polydisperse samples. At the first step of the data processing, the diffusion coefficient distribution by intensity was determined from the measured autocorrelation function, $g^{(2)}(\tau)$. Next, from the obtained intensity vs diffusivity distribition, the mass distribution of the particles (micelles) was calculated by means of the Rayleigh−Gans−Debye theory. This method has been proven to be useful in determining the mass distribution of samples with polydispersity even larger than the micelle size; moreover, this method minimizes the influence of "dust" particles.

The polydispersity index of the SDP2S micelles formed in the presence of Al^{3+} was found to be the same (the variance is between 0.3 and 0.5) as that of those formed in water solutions containing SDS and high NaCl concentrations, see ref 32. As mentioned above, the ladder model accounts for the fact that the rodlike micelles are strongly polydisperse and provides an expression, eq 1.5, for their size distribution.

The *static* light scattering technique gives the *radius of gyration* of the micelles, R_G, which is determined from the angular dependence of the scattered light.[14,32] The scattered intensity, I_S, is measured as a function of the scattering angle, θ. Next we plotted the data as I_S^{-1} vs q^2 in accordance with the equation[14,32]

$$I_S^{-1}(\theta) = I_{S_o}^{-1}(1 + {}^1/_3(R_G q)^2 + \ldots) \qquad (2.7)$$

and from the slope of the straight line, we determined R_G. This method for determining R_G is applicable for any micellar shape except for q belonging to the interval $q_{min} \le q \le q_{max}$, where $q_{min}R_G > 0.1$ and $q_{max}R_G \le 1$ (out of this interval, experimental problems appear).[32] The lowest scattering angle in our intensity measurements experiments was 30°, while the largest one depended on the size of the measured scattering objects. (q_{max} was determined from the plot of the experimental data for I_S^{-1} vs q^2: for $q > q_{max}$, the data deviated from the straight line dependence.) In all experiments, we worked with $q_{max}R_G < 0.8$. For instance, in the case of SDP2S micelles with $R_G = 45$ nm, the intensity measurements were carried out using 10−15 different scattering angles in the range 30−60°. The experimental procedure usually began with measuring the intensity at various angles in the interval 30−90°. For that purpose, we used a large round glass cell (Burchard cell, Malvern Ins., U.K.), especially designed for intensity measurements at various angles. The preliminary information for the radius of gyration of micelles helped us to choose the appropriate working range. After that, we performed at least three runs for each sample, and the final result was calculated by averaging. The influence of the intensity of the initial laser beam was also checked. For large micelles ($R_G > 10$ nm) the reproducibility of the results was very good, in the limits of 3−5%. For smaller micelles, the angular dependence was not well pronounced, and it was not possible to obtain a reliable result.

The value of the ratio $\rho_m \equiv R_G/R_H$ depends on the micelle shape and size, see, e.g., Table 1 in ref 33. It is established that, for impermeable spheres, $\rho_m = 0.775$; for monodisperse random

(31) Pusey, P. N.; Tough, R. J. A. In *Dynamic Light Scattering*; Pecora, R., Ed.; Plenum Press: London, 1985; Chapter 2.

(32) Mazer, N. A. In *Dynamic Light Scattering*; Pecora, R., Ed.; Plenum Press: London, 1985; Chapter 8.

(33) Van De Sande, W.; Persoons, A. *J. Phys. Chem.* **1985**, *89*, 404.

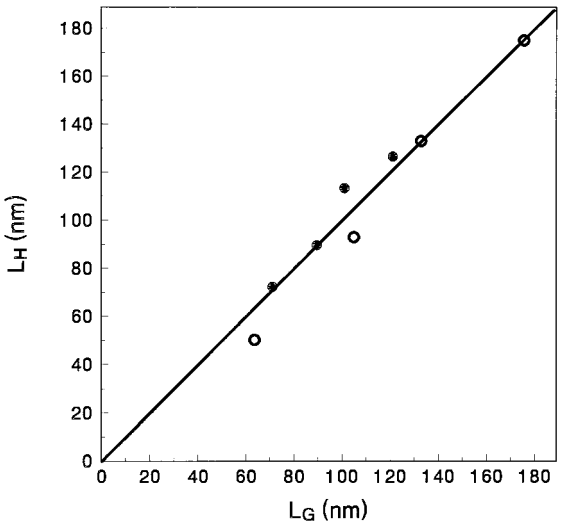

Figure 2. Plot of L_H vs L_G; the ionic strength I_0 is 24 and 64 mM for the full and empty points. L_H and L_G denote the length of a micelle calculated from the micelle hydrodynamic and gyration radius, respectively. The straight line corresponds to $L_H = L_G$.

coils, $\rho_m \approx 1.5$; and for elongated (rodlike) micelles, ρ_m varies in the range 1.35−4.01; see ref 34 and the literature quoted therein. For the solutions of SDP2S with Al^{3+}, studied by us, values $\rho_m = 1.96$ for ionic strength $I_0 = 24$ mM and $\rho_m = 2.00$ for $I_0 = 64$ mM have been experimentally obtained, see Figure 7 in ref 14. This is an indication for the rodlike shape of the micelles in these solutions. Another indication is the value of the micelle persistent length, determined in ref 14, which corresponds to a rigid rod.

To determine the length of the rodlike micelles, L, from the light scattering data (L is the sum of the length of the cylinder plus the radii of the two hemispherical caps, see Figure 1), we used the same model as in ref 14. We assumed that the *radius* of the rod is constant and equal to the radius of the smallest spherical micelles (those with $n = n_0$). On the other hand, the *length* of the rod, L, can vary with the surfactant and electrolyte concentration. L is calculated from the *time* dependence of the intensity authocorrelation function of the scattered light by using eqs 2.3−2.14 in ref 14. The value of L determined in this way (from the apparent hydrodynamic radius of the micelles) we denoted by L_H.

On the other hand, L can be independently determined from the measured radius of gyration R_G (static light scattering technique) by means of eqs 2.15, 2.16, and 3.2 in ref 14. The value of L determined in this way, we denoted by L_G. In particular, to calculate L_G we used the values of the persistent length, l_p, determined in ref 14, as follows: $l_p = 190$ nm for $I_0 = 0.024$ M and $l_p = 165$ nm for $I_0 = 0.064$ M.

In Figure 2, we plotted L_H vs L_G for solutions of SDP2S in the presence of NaCl and $AlCl_3$. The full points were measured at ionic strength $I_0 = 24$ mM, whereas the empty points were measured at $I_0 = 64$ mM; the various points correspond to different values of ξ, varying between 0.25 and 0.9. The data complies well with the line $L_H = L_G$ (Figure 2). The fact that the data for L_H vs L_G are in general agreement with the line $L_H = L_G$ for various values of ξ and I_0 shows that the determined micelle length is not sensitive to the micelle−micelle interactions in the framework of the experimental error, which can be up to 10−15%. Indeed, theoretically, L_H and L_G depend on the micelle−micelle interactions in a quite different way. (L_G and R_G depend on the interactions through the thermodynamic second virial coefficient in the expansion of the osmotic pressure, whereas L_H and R_H depend on the interactions through the kinetic second virial coefficient in the expansion of the diffusion coefficient, see, e.g., ref 32.) If there were a pronounced effect of the interactions, this in general would result in differences between the values of L_H and L_G varying with ξ and I_0, which is not the case (Figure 2).

(34) Herzog, B.; Huber, K.; Rennie, A. R. *J. Colloid Interface Sci.* **1994**, *164*, 370.

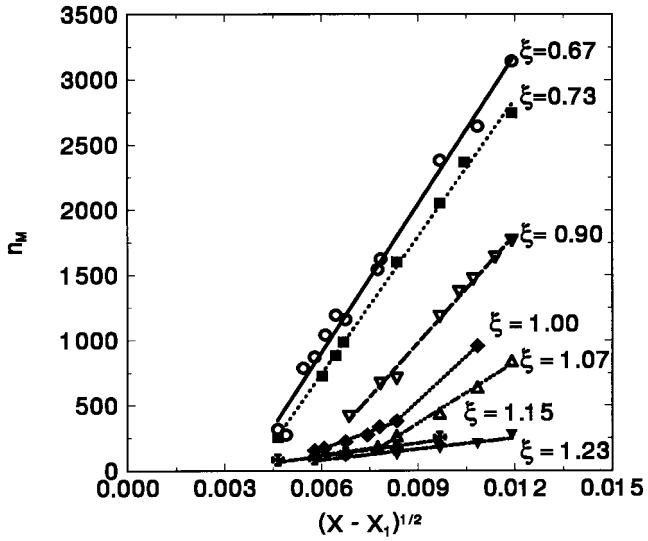

Figure 3. Data for the micellar mean mass aggregation number $\bar{n}_M$ vs $(X - X_1)^{1/2}$ at ionic strength $I_0 = 0.024$ M in the presence of Al^{3+} and Na^+. For each curve, ξ is kept constant, cf. eq 2.2; the lines are guides to the eye, rather than theoretical fits.

The above result is not surprising in view of the criterion proposed by Missel et al.[9] Comparing theory and experiment, these authors established that the micelle−micelle interactions become important only when[9]

$$\frac{X}{X^*} = \frac{R_G}{2}\left(\frac{4\pi}{3V_m}\right)^{1/3} \geq 0.45 \qquad (2.8)$$

Here R_G is the average micelle radius of gyration, $V_M = 18n_M/[(X - X_1)N_A]$, with N_A being the Avogadro number, is the average volume per micelle in the solution, X^* is the surfactant molar fraction at which the mean distance between the micelles is equal to the mean micellar radius of gyration. For the solutions investigated by us, $X/X^* \leq 0.30$, and according to eq 2.8, the micelle−micelle interactions were negligible (in first approximation). To make this estimate, we used the experimentally measured values of R_G. For example, with the largest surfactant concentration, $c_S = 8$ mM and $\xi = 0.67$, we measured $R_G = 32$ nm; for comparison, the Debye screening length (cf. eq 3.13 below) is 1 order of magnitude smaller, $\kappa^{-1} \approx 2$ nm. Thus, one may conclude that the electrostatic micelle−micelle interaction is small compared with the excluded volume interaction; the latter, in view of the criterion $X/X^* \leq 0.30$, is sufficiently small and does not affect the light scattering data. Note that additional suppression of the electrostatic micelle−micelle interaction stems from the decrease of the micelle surface charge due to the binding of Al^{3+} ions, see section 2.4 below.

We should also note that our light scattering data were not affected by multiple light scattering. Indeed, it is easy to indicate the existence of multiple light scattering because in such a case, a typical halo picture is observed in the light scattering experiment. It is due to the secondary scattered light. In all experiments carried out by us, the laser beam passing through the micellar solutions was clear without any halo. In addition, the theoretical estimates[31] also show that the multiple light scattering is negligible in the concentration range 0.05−0.3 wt % corresponding to our experiments.

2.3. Mean Mass Aggregation Number. From the radius and length of the rodlike micelles, determined as explained above, we calculated the micelle aggregation number, $\bar{n}_M$, see eq 1.7, following the procedure of ref 14, which is described in Appendix 1 below.

In Figure 3 we present the determined micellar aggregation number $\bar{n}_M$ vs $(X - X_1)^{1/2}$. Each experimental curve corresponds to a fixed value of ξ (denoted in the figure) and to a fixed ionic strength $I_0 = 24$ mM, the latter being the same for all curves. As mentioned above, experimentally we achieved a constant ξ at fixed ionic strength by diluting step by step the initial concentrated solution with a solution of NaCl of the same ionic

strength containing the surfactant of concentration equal to the cmc. The curves with $\xi = 0.90$, 1.00, and 1.15 represent new experimental data, whereas the curves with $\xi = 0.67$, 0.73, 1.07, and 1.23 were taken from Figure 5 in ref 14.

The theoretical models of micellar growth in the presence of 1:1 electrolyte[3,16] predict that the plots of $\bar{n}_M$ vs $(X - X_1)^{1/2}$ should be straight lines, see eq 1.8. The data for $\xi < 1$ really conform to straight lines (Figure 3), but this does not mean that the traditional ladder model fits the data. Indeed, the intercepts of those lines are negative (about −1300), whereas eq 1.8 predicts that the intercept must be equal to the aggregation number of the smallest spherical micelles, n_0; we experimentally determined that $n_0 \approx +56$ for SDP2S micelles. In other words, the intercepts of the straight lines for $\xi < 1$ differ in both magnitude and sign from the prediction of eq 1.8. Moreover, negative values of n_0 are physically meaningless. Other experimental curves (those with $\xi = 1.00$ and $\xi = 1.07$) are not linear at all. Therefore, one can conclude that the traditional ladder model of micelle growth[3,16] (designed for 1:1 electrolyte solutions) is not applicable (and should not be expected to be applicable) to the interpretation of data for the micellar growth in the presence of 3:1 electrolyte.

On the other hand, it should be noted that, in the absence of Al^{3+} ions (in the presence of 1:1 electrolyte only), the micelles of the investigated surfactant SDP2S grow in accordance with the prediction of the traditional ladder model (see Figure 3 in ref 35). In other words, the specific type of surfactant used in our experiment (ethoxylated alkyl sulfate) is not the reason for the difference between theory and experiment.

To interpret the data in Figure 3, we have taken into account the effect of the 3:1 electrolyte on the parameter K in eq 1.6, see section 3 below. First of all, we needed to know the fraction of Al^{3+} bound to the surface of the micelles. In this respect, useful information can be obtained by means of ultrafiltration experiments.

2.4. Ultrafiltration Experiments. As is known, the multivalent counterions bind strongly to the negatively charged surface of the anionic micelles and can be removed from the solution by performing ultrafiltration experiment using a membrane with appropriate pore size.[36,37] When the micelles are rejected by an efficient ultrafiltration membrane, all the ions belonging to the electric double layers around the micelles are retained, and the counterion concentration in the solution permeating through the pores is identical to that of the surrounding aqueous medium.

We applied this method to determine the background concentration of the unbound Al^{3+} counterions, c_{AB}, in solutions containing 2 and 8 mM SDP2S at ionic strength $I_0 = 24$ mM and at different values of the total input concentration of Al^{3+}, c_{AT}. The ultrafiltration experiments were carried out at room temperature (22 ± 2 °C) in dead-end mode in a 100-mL stirred cell. The transmembrane pressure was kept constant at 0.5 atm during the experiments. We used a polysulfonic membrane with molecular weight cut-off of 6000 which is small enough to permit the retention of the smallest SDP2S micelles. The cell was initially filled with 50 mL of the solution, and samples of 5 mL were taken throughout the run which were then used for the spectrophotometric determination of the Al^{3+} concentration in the permeate, c_{AB}. For that purpose, we used a colorimetric reaction between the ammonium salt of the aurin-tricarboxylic acid (Aluminon, Sigma) and the Al^{3+} ions taking place at low pH values.[25]

In Figure 4, we plotted the experimental data for c_{AB}/c_{SM} and c_{AB}/c_{AT} vs ξ for $c_s = 8$ mM, where $c_{SM} = c_s - \text{cmc}$ is the average concentration of the surfactant in micellar form and c_s is the total surfactant concentration. The ratio c_{AB}/c_{AT} expresses the part of the aluminum ions which are not associated with the micelles; one sees in Figure 4 that this part decreases from 32 to 11% with the increase of ξ. In other words, the predominant part of Al^{3+} ions in the investigated solutions (from 68 to 89%)

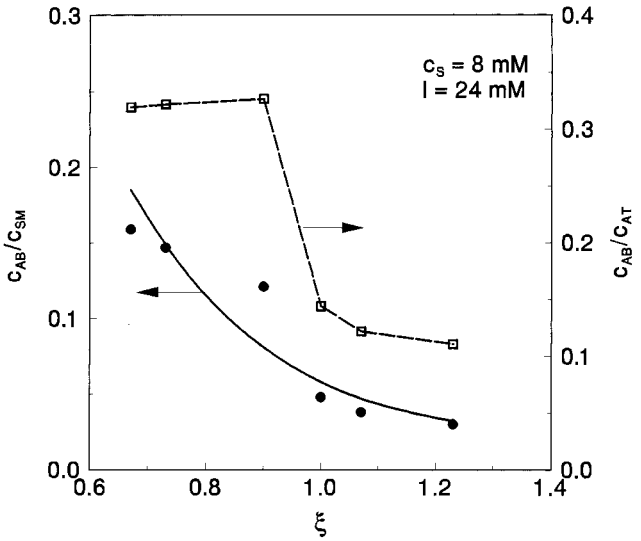

Figure 4. Plots of ultrafiltration data for c_{AB}/c_{SM} and c_{AB}/c_{AT} vs ξ for fixed $c_S = 8$ mM and $I_0 = 24$ mM. The solid line is drawn by means of eq 2.13 for $B = 0.085$ mM. The broken line for the plot of c_{AB}/c_{AT} vs ξ is a guide to the eye.

is associated with the surfactant micelles. In this aspect there is a great difference with the micelle growth in solutions of 1:1 electrolyte, when the amount of counterions associated with the micelles is negligible in comparison with the total electrolyte concentration.[3,9] To be able to interpret the data in the case when Al^{3+} ions are present, we need to know what is the background aluminum concentration, c_{AB}, corresponding to a given total aluminum concentration c_{AT}. To obtain a theoretical estimate we used the following model considerations.

The mass balance of Al^{3+} in the solution can be presented in the form

$$c_{AT} = c_{AB} + \Gamma_A a_H c_{SM} \tag{2.9}$$

where a_H is the area per headgroup of a surfactant molecule in the micelles, and Γ_A denotes the number of associated Al^{3+} ions per unit area of the micelle surface. (For simplicity, the Al^{3+} counterions belonging to the Stern and diffuse layers, see section 3.4 below, were treated in the same way.) To estimate Γ_A, we used the Langmuir adsorption isotherm

$$\Gamma_A = \Gamma_\infty \frac{c_{AB}}{B + c_{AB}}; \quad \Gamma_\infty \approx (3a_H)^{-1} \tag{2.10}$$

Here, B is a constant related to the energy of adsorption, and Γ_∞ is the maximum possible adsorption corresponding to the case when one Al^{3+} ion is bound to three surfactant headgroups. Next, in eq 2.9 we substituted Γ_A from eq 2.10 and c_{AT} from eq 2.2 (with $Z = 3$) to derive

$$3\xi x^2 + (\xi + 3E\xi - 1)x - E = 0 \tag{2.11}$$

where we introduced the notation

$$x = \frac{c_{AB}}{c_{SM}}, \quad E = \frac{B}{c_{SM}} \tag{2.12}$$

Solving eq 2.11 we obtained

$$x = \frac{1}{6\xi}\{-(\xi + 3E\xi - 1) + [(\xi + 3E\xi - 1)^2 + 12E\xi]^{1/2}\} \tag{2.13}$$

We selected the physical root of eq 2.11 which gives $x \to 0$ (no Al^{3+} in the permeate) for $\xi \to \infty$ (no Al^{3+} in solution), cf. eq 2.2. It is interesting to note that, for high surfactant concentrations when $E \to 0$ (see eq 2.12), eq 2.13 reduces to

(35) Alargova, R. G.; Ivanova, V. P.; Kralchevsky, P. A.; Broze, G.; Mehreteab, A. *Colloids Surf., A* **1998**, in press.

(36) Scamehorn, J. F.; Christian, S. D.; Ellington, R. T. *Surfactant Based Separation Processes*; J. F. Scamehorn, T. H. Harwell, Eds.; M. Dekker: New York, 1989.

(37) Hafiane, A.; Issid, I.; Lemorandt, D. *J. Colloid Interface Sci.* **1991**, *142*, 167.

$$x(\xi) = \frac{1-\xi}{3\xi} \quad \text{for} \quad \xi < 1$$
$$= 0 \quad \text{for} \quad \xi \geq 1 \tag{2.14}$$

that is, for $\xi \geq 1$, the whole amount of Al^{3+} is associated with the micelles.

We fitted the experimental data for $c_s = 2$ and 8 mM with eq 2.13 using the standard least-squares method; B was varied as an adjustable parameter. Thus, we determined $B = 8.5 \times 10^{-5}$ M from the best fit. The solid curve in Figure 4 is drawn by means of eq 2.13 with the above value of B. The agreement between theory and experiment seems quite satisfactory in view of the low accuracy of determination of c_{AB} with the colorimetric reaction and the simplifications made when deriving eq 2.13. Fortunately, it turns out that the theoretical dependence of $\bar{n}_M$ vs $(X - X_1)^{1/2}$ (see below) is not sensitive to the value of B.

3. Double Layer Contribution to the Constant of Micellization

3.1. Effect of the Counterion Adsorption on the Constant of Micellization. As already mentioned, our experimental data plotted in Figure 3 do not agree with the prediction of the available theory[3] of micelle growth, eq 1.8, at fixed constant of micellization, K. Note, however, that K can indirectly depend on the surfactant mole fraction X in the following way. As explained above, to obtain a curve *at fixed* ξ (Figure 3), we started the measurements from the most concentrated solution (8 mM SDP2S), which is further step-by-step diluted with NaCl solution of the same ionic strength, containing also SDP2S at cmc. In this way, the ratio, ξ, of surfactant-to-Al^{3+} is apparently kept constant, but more and more Na^+ is introduced into the solution. This may have the following consequences:

(i) As the energies of adsorption of Na^+ and Al^{3+} ions to the micelle surface are different, the surface charge of the micelles (and the micellization constant K) can depend on the dilution, and consequently, on the concentration c_{SM} of surfactant in micellar form.

(ii) The association of Al^{3+} with the micelles decreases the concentration of Al^{3+} in the bulk of solution ($c_{AB} < c_{AT}$, see Figure 4); consequently, the true ionic strength, I_t, of the background electrolyte is somewhat smaller than if Al^{3+} adsorption were missing. This affects the energy of the electric double layer around each micelle in solution.

Indeed, using eqs 2.12 and 2.13 and the value $B = 8.5 \times 10^{-5}$ M determined above, we calculated the dependence of c_{AB} on c_{SM} for various values of ξ. The results are presented in Figure 5 as a plot of c_{AB} vs $(X - X_1)^{1/2}$. Since the number of the water molecules in the solution is much greater than the number of the solute molecules, one may use the formula $X - X_1 \approx 0.018 c_{SM}$, where c_{SM} is expressed in mol/L. One sees that, really, the background Al^{3+} concentration, c_{AB}, depends on c_{SM}, which is more pronounced for the curves with smaller values of ξ. The symbols in Figure 5 denote the points at which measurements of the micelle aggregation number have been carried out, cf. Figure 3.

Below, we will first clarify what is the true ionic strength of the solution, I_t, and then we will consider the indirect dependence of the growth parameter, K, on c_{SM} due to the variation of I_t and c_{AB}. In other words, our aim is to check whether eq 1.8 is applicable to the interpretation of our data if the aforementioned indirect dependence of K on c_{SM} is taken into account.

3.2. True Background Concentrations of the Ionic Species. The investigated SDP2S micellar solutions contain various micro-ions, $DP2S^-$, Al^{3+}, Na^+, and Cl^-, originating from the dissolved SDP2S, $AlCl_3$, and NaCl.

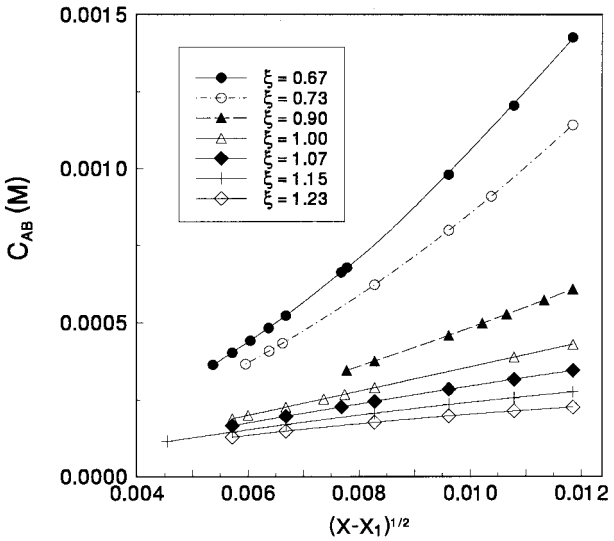

Figure 5. Theoretical curves of c_{AB} on $(X - X_1)^{1/2}$ calculated from eqs 2.12 and 2.13 for $B = 0.085$ mM and various ξ; the symbols correspond to the same values of $(X - X_1)^{1/2}$ as those of the data points in Figure 3.

In particular, SDP2S exists in the solution in both micellar and monomeric form, the concentration of the monomers being equal to cmc. Moreover, the binding of Al^{3+} to the surfactant micelles is accompanied by release of Na^+ counterions from the micelles. The background concentration of the Na^+ ions, c_{NB}, can be calculated by means of the following expression

$$c_{NB} = c_{NT} + 3(c_{AT} - c_{AB}) + [c_s - \text{cmc} - 3(c_{AT} - c_{AB})]\alpha_{Na} + \text{cmc} \tag{3.1}$$

Here c_{NT} expresses the total input concentration of Na^+ from the dissolved NaCl; the term $3(c_{AT} - c_{AB})$ stands for the Na^+ counterions replaced from the surface of each micelle by adsorbed Al^{3+} ions; the next term, $[c_s - \text{cmc} - 3(c_{AT} - c_{AB})]\alpha_{Na}$, accounts for the Na^+ ions dissociated from the micelle headgroups, which are not occupied by adsorbed Al^{3+}; α_{Na} denotes the average degree of charging of the micelle headgroups free of adsorbed Al^{3+} ($0 < \alpha_{Na} < 1$); the fact that α_{Na} is less than 1 accounts for adsorption of Na^+ ions at the micelle surface; finally, the term cmc in eq 3.1 stands for the Na^+ ions dissociated from the free surfactant monomers in the solution. As mentioned earlier, in our experiments the apparent ionic strength of the input electrolyte (NaCl and $AlCl_3$), I_0, is kept constant, $I_0 \equiv 24$ mM

$$c_{NT} + 6c_{AT} = I_0 \equiv \text{const} \tag{3.2}$$

Next, the true background ionic strength of the solution can be calculated

$$I_t = {}^1/_2(9c_{AB} + c_{NB} + 3c_{AT} + c_{NT} + \text{cmc}) \tag{3.3}$$

The term $3c_{AT} + c_{NT}$ expresses the concentration of the Cl^- ions dissociated from the dissolved $AlCl_3$ and NaCl, and the last term (cmc) in eq 3.3 accounts for the presence of ionized surfactant monomers in the solution. The substitution of c_{NB} and c_{NT} from eqs 3.1 and 3.2 into eq 3.3 yields

$$I_t = I_0 + 3c_{AB} - 3c_{AT} + \text{cmc} + {}^1/_2(c_s - \text{cmc} - 3c_{AT} + 3c_{AB})\alpha_{Na} \tag{3.4}$$

In our calculations we took into account also the fact that the critical micellization concentration (cmc) depends on the ionic strength, see eq 2.1

$$c_{SM} = c_s - \mathrm{cmc}(I_t); \quad c_{SM}{}^0 = c_s - \mathrm{cmc}(I_0); \quad c_{AT} = \frac{c_{SM}{}^0}{3\xi} \tag{3.5}$$

Let us mention in advance that for the solutions studied by us, the true ionic strength, I_t, calculated from eq (3.4), appears to be close to $I_0 = 24$ mM and is not sensitive to the variation of ξ. Moreover, $\mathrm{cmc}(I_0) \approx 0.1$ mM is too low compared to I_0 and, therefore, gives a negligible contribution to I_t.

3.3. Energy Contribution Due to the Diffuse Electric Double Layer. The energy of the electric double layer formed around a micelle gives a contribution to the standard chemical potential of a surfactant molecule incorporated into such a micelle[3] and, consequently, to the equilibrium constant K, see eq 1.6. Following refs 3 and 9, we assumed that the double-layer and nondouble-layer contributions to the standard chemical potentials are additive, and then from eq 1.6 one obtains[3,9]

$$K = K_{dl}K_{ndl} \tag{3.6}$$

where by definition

$$\ln K_{dl} \equiv \frac{n_0(g_s^{el} - g_c^{el})}{kT} \tag{3.7}$$

Here K_{dl} and K_{ndl} denote the double-layer and nondouble-layer contributions into the equilibrium constant K; g^{el} represents the electrostatic energy per surfactant molecule incorporated into a micelle. Here and hereafter, the indices "s" and "c" denote "spherical" and "cylindrical" micelle, respectively. Theoretical expressions for g^{el} have been derived by Mitchell and Ninham[19] and Missel et al.[9] for the case of a symmetrical (1:1) electrolyte. Our aim below is to derive an expression for g^{el} for the case when a mixture of 1:1 and 3:1 electrolytes (NaCl and $AlCl_3$) is present in the solution. The energy g^{el} can be calculated by means of the expression[19,38]

$$g^{el} = \frac{e}{|\sigma|}\int_0^{\sigma} \psi_0 \, d\sigma \tag{3.8}$$

where e is the elementary charge, σ denotes the surface charge density, and ψ_0 is the surface potential. To determine the dependence $\psi_0(\sigma)$, we have to solve the Poisson equation

$$\frac{d^2\psi}{dr^2} + \frac{m}{r}\frac{d\psi}{dr} = -\frac{4\pi}{\epsilon}\rho(r), \quad m = 0, 1, 2 \tag{3.9}$$

Here ψ and ρ are the electric potential and bulk charge density, respectively, and r is the coordinate along the normal to the charged surface; $m = 0$ for flat surface, $m = 1$ for cylindrical, and $m = 2$ for spherical surface. ρ can be expressed by means of the Boltzmann equation

$$\rho = ec_{NB}\exp\left(-\frac{e\psi}{kT}\right) + 3ec_{AB}\exp\left(-\frac{3e\psi}{kT}\right) - e(c_{NB} + 3c_{AB})\exp\left(\frac{e\psi}{kT}\right) \tag{3.10}$$

where, as usual, c_{NB} and c_{AB} are the background concentrations of Na^+ and Al^{3+}. Combining eqs 3.9 and 3.10 one can derive

$$\frac{d^2y}{dx} + \frac{m}{x}\frac{dy}{dx} = \sinh y = 6\lambda^2 \exp(y)\sinh^2 y \tag{3.11}$$

where we have introduced the notation

$$x = \kappa r, \quad y = -\frac{e\psi}{kT} \tag{3.12}$$

$$\kappa^2 = \frac{8\pi e^2 I_t}{\epsilon kT}, \quad \lambda^2 = \frac{c_{AB}}{I_t} \tag{3.13}$$

The boundary condition at the charged surface is $d\psi/dr = -4\pi\sigma/\epsilon$; in the above notation this equation takes the form

$$\frac{dy}{dx} = \frac{4\pi\sigma e}{\epsilon kT\kappa} \equiv -s \qquad \text{for } x = \kappa R \tag{3.14}$$

The latter equation defines the parameter s. Following the procedure of Wiersmaa et al.,[39] which has been also utilized by other authors,[9,19,40] we multiply eq 3.11 by dy/dx, integrate, and then set $y = 0$ and $y' = 0$ for $x \to \infty$; the result is

$$\left(\frac{dy}{dx}\right)^2 = 4\sinh^2\frac{y}{2} + \lambda^2(e^y - 1)^3(1 + 3e^{-y}) + \int_x^{\infty}\frac{2m}{x}\left(\frac{dy}{dx}\right)^2 dx \tag{3.15}$$

Let us denote

$$y_0 = y|_{x=\kappa R} \tag{3.16}$$

Then we use the approximation[9,19,39,40]

$$\int_{\kappa R}^{\infty}\frac{1}{x}\left(\frac{dy}{dx}\right)^2 dx \approx -\frac{1}{\kappa R}\int_0^{y_0}\frac{dy}{dx}\,dy \tag{3.17}$$

To estimate the last integral, we substitute dy/dx for a flat interface ($m = 0$). Using some appropriate approximations from eq 3.15 (with $m = 0$) we derive

$$-\int_0^{y_0}\frac{dy}{dx}\,dy \approx 8\sinh^2\frac{y_0}{4} + \lambda J(u) \tag{3.18}$$

where

$$u = [\exp(y_0) - 1]^{1/2} \tag{3.19}$$

$$J(u) \equiv {}^2/_3u^3 + u - {}^5/_2(\arctan u) + {}^3/_2u/(1 + u^2) \tag{3.20}$$

Next, the combination of eqs 3.14−3.19 yields

(38) Verwey, E. J. W.; Overbeek, J. Th. G. *Theory of the Stability of Lyophobic Colloids*; Elsevier: Amsterdam, 1948.

(39) Wiersmaa, P. H.; Loeb, A. H.; Overbeek, J. Th. G. *J. Colloid Interface Sci.* **1966**, *22*, 78.

(40) Chew, W. C.; Sen, P. N. *J. Chem. Phys.* **1982**, *77*, 2042.

$$s = \left\{4 \sinh^2 \frac{y_0}{2} + \lambda^2 u^6 (1 + 3e^{-y_0}) + \frac{2m}{\kappa R}\left[8 \sinh^2 \frac{y_0}{4} + \lambda J(u)\right]\right\}^{1/2} \quad (3.21)$$

Note that for $\lambda = 0$ (no Al^{3+} ions in the solution), eq 3.21 reduces to the respective expression of Mitchell and Ninham[19] for 1:1 electrolyte. Next, we calculate g^{el} by means of the expression

$$\frac{g^{el}}{kT} = \frac{e}{|\sigma|} \frac{kT}{e^2} \frac{\epsilon\kappa}{4\pi} (y_0 s - \int_0^{y_0} s \, dy_0) \quad (3.22)$$

which follows from eqs 3.8, 3.12, and 3.14. The integration in eq 3.22 is carried out numerically along with eqs 3.19−3.21. To obtain K_{dl} by means of eq 3.7, we calculated the values of g^{el} for spherical ($m = 2$) and cylindrical ($m = 1$) micelle; details about the procedure of calculations are given in Appendix 2.

3.4. Model of the Stern Layer. Here, we follow the traditional model of the double-layer structure.[41,42] In other words, the micelle electric double layer is supposed to consist of two parts: (i) the *diffuse layer*, which contains free counterions involved in Brownian motion and (ii) the *Stern layer* consisting of counterions which are adsorbed (bound) to the micelle surface.[41−45]

The area per surfactant headgroup, a, calculated from the results for the micelle shape and aggregation number (see Appendix 1), is $a_s = 1.48$ nm^2 for the spherical micelles and $a_c = 0.64$ nm^2 for the cylindrical ones. These values are markedly larger than the area per molecule in a dense flat surfactant adsorption monolayer, which is ca. 0.35 nm^2. Therefore, it is possible for some Al^{3+} ions to be intercalated among the surfactant headgroups at the micelle surface, thus, partially neutralizing the surface charge of the micelles (Figure 6). In such a case

$$\sigma = -\alpha \frac{e}{a} \quad (3.23)$$

where α is an *apparent* degree of dissociation (charging) of the ionizable headgroups on the surface of a micelle ($0 < \alpha < 1$). The parameter α expresses the fraction of the "nonneutralized" headgroups

$$\alpha = 1 - \theta_A - \theta_N \quad (3.24)$$

where θ_A and θ_B are the occupancies of the Stern layer by Al^{3+} and Na^+ ions[43]

$$\theta_N = \frac{b_N c_{NB}}{1 + b_N c_{NB} + b_A c_{AB}}, \qquad \theta_A \equiv \frac{3\Gamma_A}{\Gamma_s} = \frac{b_A c_{AB}}{1 + b_N c_{NB} + b_A c_{AB}} \quad (3.25)$$

Γ_s and Γ_A denote adsorption of surfactant and Al^{3+}; the multiplier 3 accounts for the fact, that one Al^{3+} ion neutralizes three surfactant headgroups. In fact, eqs 3.25 represent Langmuir isotherms for the competitive adsorption of Al^{3+} and Na^+ in the Stern layer. The adsorption parameters in eqs 3.25 are to be determined from the expressions[43,44]

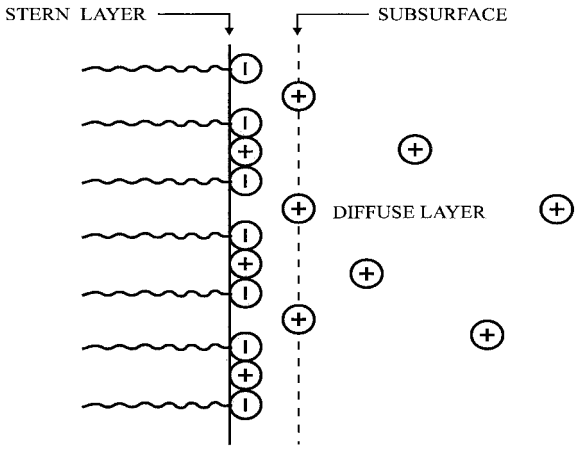

Figure 6. Sketch of the Stern layer.

$$b_N = a\delta_N \exp\left(\frac{\Phi_N + y_0}{kT}\right), \quad b_A = a\delta_A \exp\left(\frac{\Phi_A + 3y_0}{kT}\right) \quad (3.26)$$

Here a ($= a_s$ or a_c) is the area per surfactant headgroup; $\delta_N = 0.72$ nm and $\delta_A = 9.6$ nm are the diameters of the hydrated Na^+ and Al^{3+} ions; Φ_N and Φ_A are the specific adsorption energies of the respective ions. For high adsorption energy $\Phi_N \to \infty$ (or $\Phi_A \to \infty$), eqs 3.25 and 3.26 predict $\theta_N \to 1$ (or $\theta_A \to 1$), as it could be expected.

To estimate Φ_N and Φ_A we used the following model. In general, Φ_A is the work carried out to bring an Al^{3+} ion from the subsurface to the surface. The points A, B, and C in Figure 7 denote the positions of three neighboring headgroups at the surface of a micelle; D denotes the position of an Al^{3+} ion in the subsurface, and P is the position of this ion when it is intercalated among the headgroups. Then we use the Coulombic law to estimate the work carried out to bring the Al^{3+} ion from point D to point P; thus we obtained

$$\Phi_A = \frac{9e^2}{\epsilon_{st} kT}\left(\frac{1}{r_a} - \frac{1}{\sqrt{r_a^2 + \delta^2}}\right), \quad r_a = \sqrt{\frac{2a}{3\sqrt{3}}} \quad (3.27)$$

Here, δ is the distance between points D and P (the thickness of the Stern layer), and r_a (see Figure 7) is estimated, assuming hexagonal packing of the surfactant headgroups; ϵ_{st} is the dielectric constant in the Stern layer, which is expected to be different (smaller) from the dielectric constant of the bulk water because of the water molecules belonging to the hydration shells around the ions.[30,45] Likewise, one obtains an expression for Φ_N

$$\Phi_N = \frac{3e^2}{\epsilon_{st} kT}\left(\frac{1}{r_a} - \frac{1}{\sqrt{r_a^2 + \delta^2}}\right) \quad (3.28)$$

Now we have all of the equations necessary to calculate g^{el} and K_{dl}, cf. eqs 3.6 and 3.7. The procedure of calculations is described in Appendix 2.

4. Numerical Results and Discussion

4.1. Processing of the Experimental Data. The aim of the numerical procedure is to fit the experimental data from Figure 3 plotted as $\bar{n}_M$ vs $[K_{dl}(X - X_1)]^{1/2}$

(41) Stern, O. *Ztschr. Elektrochem.* **1924**, *30*, 508.
(42) Davies, J. T.; Rideal, E. K. *Interfacial Phenomena*; Academic Press: London, 1963; p 85.
(43) Derjaguin, B. V. *Theory of Stability of Colloids and Thin Films*; Plenum Press: New York, 1989.
(44) Shchukin, E. D.; Pertsov, A. V.; Amelina, E. A. *Colloid Chemistry*; Moscow University Press: Moscow, 1982. (In Russian.)
(45) Adamson, A. W. *Physical Chemistry of Surfaces*; Wiley: New York, 1976.

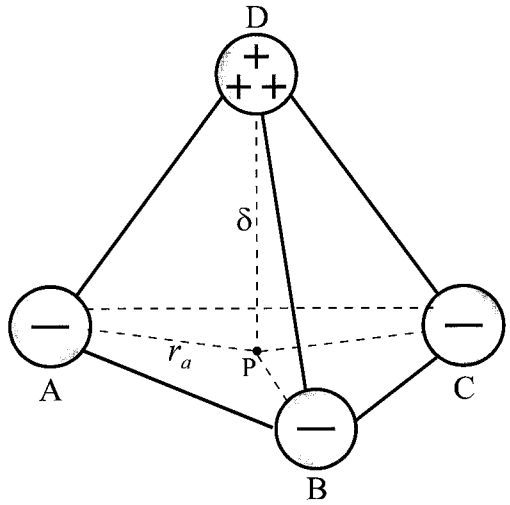

Figure 7. Model used to derive the energy of adsorption, eq 3.27. A, B, and C denote the positions of three surfactant headgroups; D and P denote the positions of an Al^{3+} counterion in the subsurface and among the headgroups, respectively.

$$\bar{n}_M = n_0 + [2\sqrt{K_{ndl}}]t; \quad t \equiv [K_{dl}(X - X_1)]^{1/2} \quad (4.1)$$

Equation 4.1 is a corollary of eqs 1.8 and 3.6. $\bar{n}_M$ is given by the experiment. In addition, $X - X_1 = 0.018(c_s - \text{cmc}) = 0.018c_{SM}$ where the values of c_s and cmc (in mol/L) are also known from the experiment; see also eqs 2.1 and 3.5. The aggregation number of the smallest spherical micelles is also known from the experiment: $n_0 \approx 56$. The equations from the previous section allow the calculation of K_{dl} for a given value of X (see Appendix 2). As K_{ndl} is not expected to depend on X, eq 4.1 shows that the plot of $\bar{n}_M$ vs t should be a straight line. To fit the data, we apply the least-squares method by minimization of the function

$$\Psi(\delta, K_{ndl}) = \sum_i [(\bar{n}_M)_i - \bar{n}_M(t_i)]^2 \quad (4.2)$$

where $(\bar{n}_M)_i$ and t_i are values of $\bar{n}_M$ and t calculated from the experimental data; $\bar{n}_M(t_i)$ is calculated by means of eq 4.1 and the summation is carried out over all experimental points. From the best fit of the data for $\xi = 0.67$ (see the respective curve in Figure 3) with eq 4.1, we determine $\delta = 4.6$ Å and $K_{ndl} = 1.08 \times 10^7$. The data (the full circles in Figure 8) comply well with a straight line of intercept $n_0 = 56$.

We applied the same numerical procedure (based on eq 4.2) to process the data for the other values of ξ ($0.73 \le \xi \le 1.23$). It turns out that, for these data, the minimum of Ψ vs K_{ndl} is rather shallow (flat), and therefore, the value of K_{ndl} determined by the minimization procedure is rather uncertain. (On the other hand, the minimum of Ψ vs δ is very well pronounced.) We solved the problem in the following way.

Since K_{ndl} is not expected to depend on ξ, we fixed the value $K_{ndl} = 1.08 \times 10^7$, determined for $\xi = 0.67$, and processed the data for the other values of ξ ($0.73 \le \xi \le 1.23$, see Figure 3) with a single adjustable parameter, δ. The values of δ determined from the best fits are listed in Table 1; all of them are between 4.1 and 4.6 Å, which is a physically reasonable result. The slight decrease of δ with the rise of ξ could be attributed to the increasing "weight" of the spherical micelles when the average micelle size decreases (as mentioned earlier, the area per headgroup is larger for the spherical micelles, for which a smaller δ can be expected).

Table 1. Parameter Values Determined from the Fit in Figure 8 for Various Surfactant-to-Al^{3+} Ratio ξ[a]

ξ	δ (Å)	$\Phi_A{}^c$ (kT)	$\Phi_A{}^s$ (kT)	$\Phi_N{}^c$ (kT)	$\Phi_N{}^s$ (kT)
0.67	4.60	4.78	1.72	1.60	0.57
0.73	4.58	4.76	1.71	1.59	0.57
0.90	4.50	4.65	1.66	1.55	0.55
1.00	4.37	4.48	1.59	1.49	0.53
1.07	4.34	4.44	1.57	1.48	0.52
1.15	4.18	4.22	1.48	1.41	0.49
1.23	4.14	4.17	1.45	1.39	0.48

[a] The superscripts c and s denote cylindrical and spherical micelles, respectively.

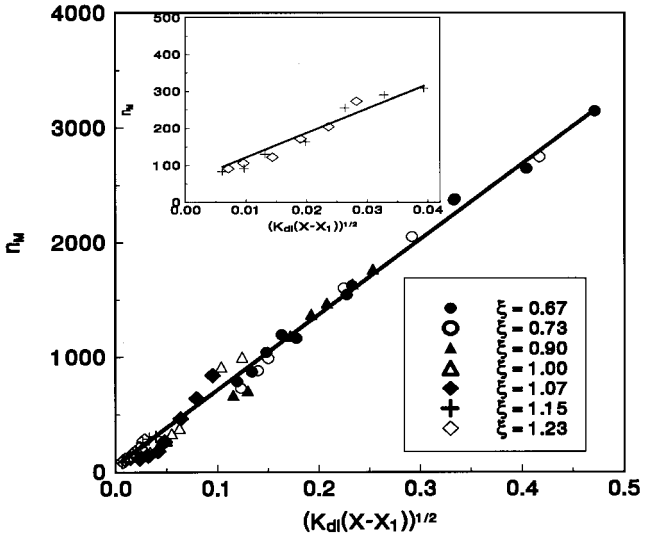

Figure 8. The data from Figure 3 plotted in accordance with eq 4.1. The inset shows the data for $\xi = 1.15$ and 1.23 in an enlarged scale. The straight line corresponds to $\delta = 4.6$ Å, $K_{ndl} = 1.08 \times 10^7$ and $n_0 = 56$.

One sees in Figure 8 that the data from all of the curves in Figure 3, corresponding to $0.67 \le \xi \le 1.23$, are in general agreement with the *same* straight line with intercept and slope corresponding to $n_0 = 56$ and $K_{ndl} = 1.08 \times 10^7$, see eq 4.1. This result means that the model of micelle growth by Missel et al.[3] is applicable to our experimental system if the effect of electrolyte on K_{dl} is accounted for as shown in section 3 above.

It should be noted, that all data are processed with the same value of the dielectric constant of the Stern layer: $\epsilon_{st} = 55.5$. This value provides the best fit of our data for Al^{3+} ions and new data for Ca^{2+} ions.[35] The value $\epsilon_{st} = 55.5$ seems acceptable in so far as it is between $\epsilon = 78.3$ for the bulk water and $\epsilon \approx 32$ for the hydration shells of the ions.[30,45]

4.2. Physical Cause for the Micelle Growth. Processing the experimental data for $\bar{n}_M$ vs $t \equiv (K_{dl}(X - X_1))^{1/2}$ (see Figure 8), we calculated the values of many physical parameters (such as adsorption energy, micelle surface charge and potential, electrostatic energy per monomer, etc.) which reveal the physical picture and cause of the micelle growth in the investigated system.

Let us start with the adsorption energies, Φ_A and Φ_N, calculated by means of eqs 3.27 and 3.28. Since the areas per headgroup for the cylindrical and spherical micelles are different ($a_c = 0.64$ nm^2; $a_s = 1.48$ nm^2, see Appendix 1), the respective values of Φ_A and Φ_N are different, see Table 1 and eqs 3.27−3.28; it turns out that the energy of adsorption at a cylindrical micelle is about 2.8 times larger than that at a spherical micelle. In addition, for micelles of the same shape, Φ_A is 3 times larger than Φ_N due to the 3-fold larger charge of Al^{3+} as compared to Na^+.

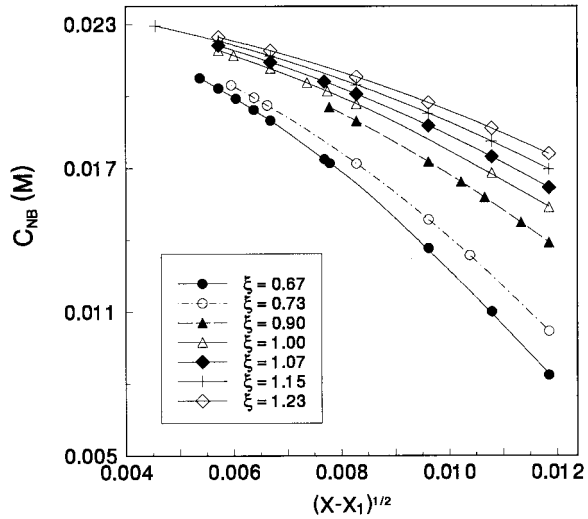

Figure 9. Theoretical plot of the Na^+ background concentration c_{NB} vs $(X - X_1)^{1/2}$ for various values of the surfactant-to-Al^{3+} ratio ξ; the symbols correspond to the same values of $(X - X_1)^{1/2}$ as those of the data points in Figure 3.

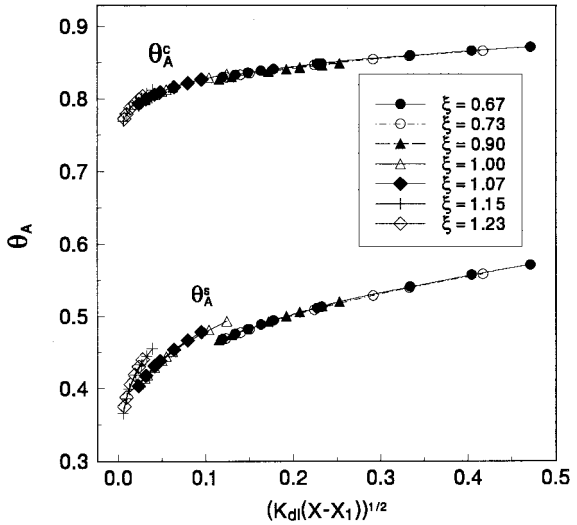

Figure 10. Calculated occupancy of the Stern layer by Al^{3+} ions for cylindrical and spherical micelles: θ^c_A and θ^s_A, respectively, plotted vs $(K_{dl}(X - X_1))^{1/2}$; the symbols correspond to the same values of $(X - X_1)^{1/2}$ as those of the data points in Figure 3.

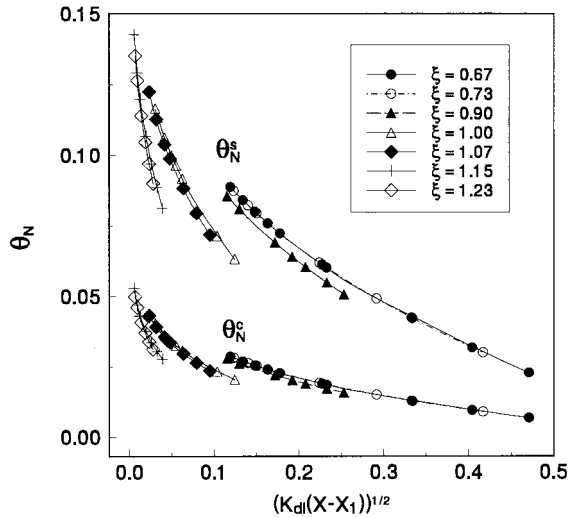

Figure 11. Calculated occupancy of the Stern layer by Na^+ ions for cylindrical and spherical micelles: θ^c_N and θ^s_N, respectively, plotted vs $(K_{dl}(X - X_1))^{1/2}$; the symbols correspond to the same values of $(X - X_1)^{1/2}$ as those of the data points in Figure 3.

Figure 9 shows the background concentration of Na^+, c_{NB}, calculated by means of eq 3.1 (see Appendix 2 for details). The symbols in Figure 9 denote the points at which measurements of the micelle aggregation number have been carried out, see Figures 3 and 8. One sees that at the lower surfactant concentrations, c_{NB} is close to $I_0 = 0.024$ M, i.e., practically the whole ionic strength of the solution is due to the Na^+ ions. With the increase of surfactant concentration at fixed ξ and ionic strength (see eqs 2.2 and 3.2), the Na^+ ions are replaced by Al^{3+} ions, and c_{NB} decreases. In spite of the lower adsorption energy of the Na^+ ions ($\Phi_N < \Phi_A$, see Table 1), they can compete with Al^{3+} for the adsorption in the Stern layer, especially at the lower values of $X - X_1$, at which c_{NB} is larger than c_{AB}, cf. Figures 5 and 9. The true ionic strength of the solutions, I_t, calculated from eq 3.4, is very close to $I_0 =$ 24 mM for the lowest surfactant concentration ($c_s = 2$ mM), and it monotonically decreases down to 17−19 mM (depending on ξ) for the highest investigated surfactant concentration, $c_s = 8$ mM. Concerning the screening of the micelle electric potential, this variation of I_t is not significant in so far as the Debye screening parameter κ is proportional to $I_t^{1/2}$, see eq 3.13. It turns out that the variation of the surface charge of the micelles is more important, see below.

Figure 10 presents the occupancy, θ_A, of the Stern layer by Al^{3+} as a function of $t \equiv (K_{dl}(X - X_1))^{1/2}$ for the cases of cylindrical and spherical micelles and for various ξ. It is not surprising that θ_A is greater for the cylindrical micelles because the distances between their surfactant headgroups are smaller, and consequently $\Phi_A{}^c > \Phi_A{}^s$, see Table 1. The increase of θ_A with the surfactant concentration can be attributed to the increase of the bulk Al^{3+} concentration with the rise of $X - X_1$, see Figure 5. At the larger surfactant concentrations, θ_A approaches 87% for the cylindrical micelles, which means that the micelle surface charges are neutralized to a great extent and that there is not much space left in the Stern layer for the adsorption of Na^+ ions.

Figure 11 shows the occupancy, θ_N, of the Stern layer by Na^+ ions. The latter may occupy adsorption sites free of Al^{3+}, and that is the reason why θ_N is larger for the spherical micelles, which bind less Al^{3+} than the cylindrical ones, cf. Figure 10. Anyway, in these experiments, θ_N may increase up to 15% (Figure 11), and it should not be neglected when calculating the micelle surface charge.

Figure 12 presents the calculated degree of charging α of the cylindrical and spherical micelles, see eq 3.24. One sees that α decreases with the rise of $X - X_1$ which is due to the fact that the background Al^{3+} concentration, c_{AB}, and θ_A increase together with $X - X_1$, see Figures 5 and 10. For the spherical micelles, θ_A varies between 40 and 50%; whereas for the cylindrical ones, θ_A is between 12 and 18%.

It is interesting to note that, unlike the surface charge, the calculated surface potential is almost the same for the spherical and cylindrical micelles at the same surfactant concentrations. The dimensionless micelle surface potential, y_0, cf. eq 3.12 and 3.16, decreases from 2.5 to 1.6 with the rise of surfactant concentration.

The fact that the spherical micelles are markedly more charged as compared to the cylindrical ones, see Figure 12, is very important for the understanding of the physical cause of the micelle growth. The fact is that $\alpha_s > \alpha_c$ leads to a greater electrostatic energy per monomer in the spherical micelles, $g^{el}{}_s > g^{el}{}_c$. The difference $g^{el}{}_s - g^{el}{}_c$

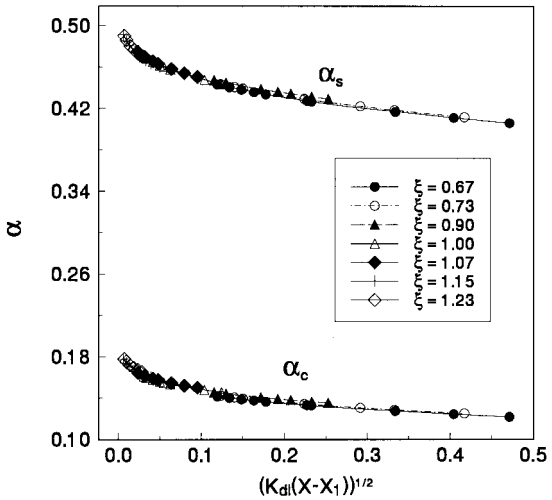

Figure 12. Calculated degree of charging, see eq 3.24, for cylindrical and spherical micelles: α_c and α_s respectively, plotted vs $(K_{dl}(X - X_1))^{1/2}$; the symbols correspond to the same values of $(X - X_1)^{1/2}$ as those of the data points in Figure 3.

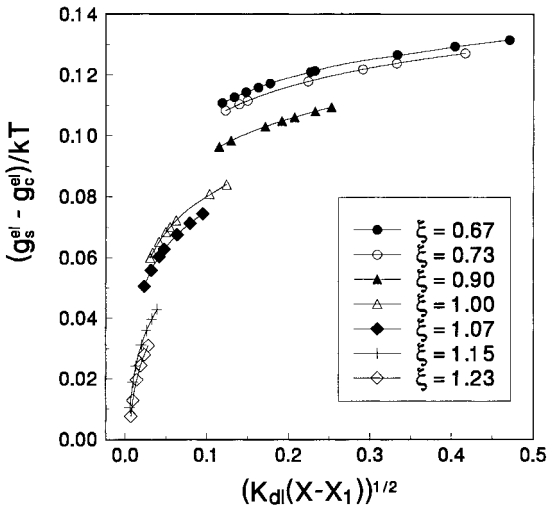

Figure 13. Calculated difference between the electrostatic energies of a surfactant monomer incorporated in a spherical and cylindrical micelle, $g^{el}{}_s$ and $g^{el}{}_c$, respectively, plotted vs $(K_{dl}(X - X_1))^{1/2}$ for various ξ; the symbols correspond to the same values of $(X - X_1)^{1/2}$ as those of the data points in Figure 3.

is plotted vs $t \equiv (K_{dl}(X - X_1))^{1/2}$ in Figure 13. One sees that $g^{el}{}_s - g^{el}{}_c$ increases with the increase of the surfactant concentration, $X - X_1$, and with the decrease of ξ. The mean aggregation number of the micelles, $\bar{n}_M$, behaves in the same way, cf. Figure 3. In other words, the formation of larger cylindrical micelles is energetically more favorable because they bear a lower surface charge, and consequently, they have lower electric energy (per monomer) than the spherical micelles. In our case $g^{el}{}_s - g^{el}{}_c$ is less than 0.14 kT (Figure 13), whereas $g^{el}{}_s$ and $g^{el}{}_c$, separately, are about 10 times larger (from 1 to 1.5 kT).

In spite of the fact that the difference $g^{el}{}_s - g^{el}{}_c$ is relatively small (as compared to $g^{el}{}_s$ or $g^{el}{}_c$), it affects strongly the micellization parameter K_{dl} because it enters eq 3.7 multiplied by the aggregation number $n_0 \approx 56$. Figure 14 shows the calculated micellization parameter $K = K_{dl}K_{ndl}$ vs $(X - X_1)^{1/2}$. It turns out that for the investigated solutions, the plots are straight lines, which are different for the different values of ξ. Note that the variation of K is, in fact, due to the variation of K_{dl}, because, as mentioned earlier, the nondouble-layer contribution

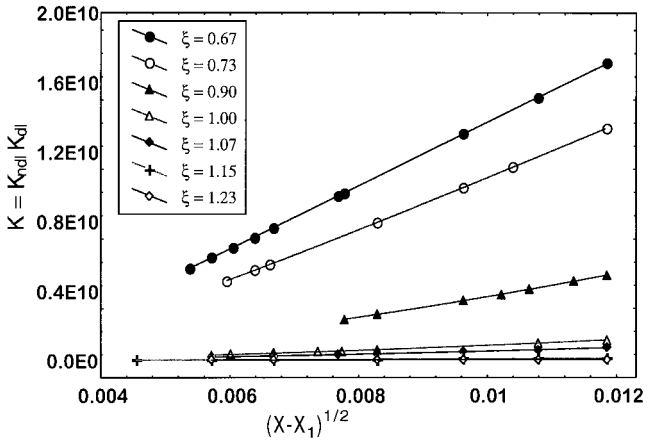

Figure 14. Calculated equilibrium constant, K, plotted vs $(X - X_1)^{1/2}$ for various ξ; the symbols correspond to the experimental points in Figure 3, see Appendix 2 for the procedure of calculations; the symbols correspond to the same values of $(X - X_1)^{1/2}$ as those of the data points in Figure 3.

into K is expected to be independent of the surfactant and electrolyte concentrations and is determined to be $K_{ndl} = 1.08 \times 10^7$.

4.3. Discussion about the Importance of the Electrostatic Effects. Finally, let us come back to the discussion about the importance of the two types of electrostatic effects in micellar solutions of ionic surfactants as formulated in the Introduction: (i) *electrostatic energy of micellization* and (ii) *electrostatic interaction between the micelles*. The whole of our analysis in this study shows that effect (i), rather than effect (ii), is the decisive factor influencing the micelle growth in the presence of Al^{3+} ions in the investigated range of solute concentrations. Quantitatively, the most important factor influencing the micelle growth turns out to be the binding of Al^{3+} counterions to the micelle surface, which has a very strong effect on the value of the micellization constant, K. The latter can vary by orders of magnitude when the bulk concentration of Al^{3+} (and the parameter ξ) is varied, see eqs 2.2 and 3.6−3.7 and Figures 13 and 14.

On the other hand, effect (ii), i.e., the electrostatic interaction between the micelles, turns out to have a negligible influence on the micelle growth. Below, we summarize the arguments in favor of the latter conclusion:

(a) As stated in the discussion after eq 2.8 above, in our case, the electrostatically driven nonidealities in the micellar solutions are much smaller than the sterically driven nonidealities ($\kappa^{-1} \approx 2$ nm, whereas $L_H \approx$ dozens of nm).

(b) The situation with the micellar solutions with Na^+ ions studied by Missel et al.[3] is similar, i.e., the steric nonidealities are predominant. Their importance for the micellar growth can be estimated by means of the criterion, eq 2.8 above, which was derived by Missel et al.[9] The latter authors worked with expressions for an ideal solution because in their case, $X/X^* \leq 0.4$, see p 8359 in ref 9. In our case, the nonidealities should be even smaller in so far as for our solutions $X/X^* \leq 0.3$. In other words, following ref 9, we can also claim that the nonidealities in our micellar solutions do not essentially affect the micelle growth.

(c) In addition to the X/X^* criterion, and independently from it, we compared experimental data for L_G and L_H, which again show that the micelle−micelle interactions do not essentially affect the micelle size distribution, see Figure 2 and the related discussion.

(d) A fourth argument in favor of the negligibility of the micelle−micelle interactions is the general agreement of

the experimental data with the theoretical line (based on eq 1.1), see Figure 8 above. Note that Figure 8 contains 49 experimental points obtained at *various* concentrations of surfactant and Al^{3+} and Na^+ ions, all of them complying with the same theoretical line, drawn by varying only two adjustable parameters, δ and K_{ndl}. Moreover, we have determined the values $\delta = 4.6$ Å and $K_{ndl} = 1.08 \times 10^7$ only from the data with $\xi = 0.67$, and it turns out that the data for all other ξ ($0.73 \leq \xi \leq 1.23$) conform to the same fit without adjusting any parameter. Of all, the intercept of the theoretical line (Figure 8) gives the correct value of the aggregation number of the spherical micelles, $n_0 \approx 56$. We believe this agreement between the theoretical model and the experimental data is not fortuitous.

The above arguments lead us believe that the theoretical model proposed by us (an extension of the ladder model) is, in general, adequate to the experimental situation.

5. Conclusions

This work was provoked by the finding[14] that there is no adequate theory for interpreting experimental data for the growth of rodlike micelles in the presence of 3:1 electrolyte. The available ladder model by Missel et al.[3] is originally designed for 1:1 electrolyte. To solve the problem, we undertook additional experimental and theoretical investigations. In particular, we demonstrated that the ladder model can be extended to 3:1 electrolytes.

First of all, we gathered additional dynamic light scattering data, see the lines with $\xi = 0.90$, 1.00, and 1.15 in Figure 3. The new data confirm the finding in ref 14 that the micellar growth in the presence of Al^{3+} does not obey eq 1.8 at fixed K. In addition, the results of independent dynamic and static light scattering measurements imply that the effect of the micelle−micelle interactions on the measured diffusion coefficient and mean mass aggregation number, $\bar{n}_M$, can be neglected (in first approximation) for the surfactant and electrolyte concentrations used, see Figure 2 and eq 2.8.

We carried out ultrafiltration experiments which revealed that the predominant part (from 68 to 89%) of Al^{3+} is associated with the micelles (Figure 4). We derived an expression, eq 2.13, which allows estimating the concentration, c_{AB}, of Al^{3+} remaining in the background solution at a given surfactant concentration, c_s, see Figure 5.

The latter dependence of c_{AB} on c_s turns out to be crucial for the interpretation of the experimental data. Indeed, the equilibrium constant, K, depends on c_{AB}, and in addition, c_{AB} increases with the rise of c_s at fixed ξ, see Figure 5. This leads to an indirect dependence of K on c_s. It turns out that to check whether our experimental data complies with the ladder model, eq 1.8, one should derive the theoretical dependence of K vs c_s. This is done in section 3; see also Figure 14. The comparison of the theory with the experiment shows a good agreement. In particular, the data from all curves in Figure 3 are in general agreement with a single straight line in Figure 8 as predicted by the ladder model, complemented with the theory from section 3, see eq. 4.1.

Experimentally we achieved constant ξ at fixed ionic strength by diluting step by step the initial concentrated surfactant solution with solution of NaCl of the same ionic strength containing surfactant of concentration equal to the cmc. The theoretical results from section 3 allowed us to understand what happens with the micelles in the solution when the latter is diluted. The resulting physical picture is the following:

(i) The decrease of the surfactant concentration in these experiments is accompanied by a decrease of the background Al^{3+} concentration (Figure 5).

(ii) This leads to a decrease of the Al^{3+} adsorption in the micelle Stern layer (Figure 10) and to the increase of the surface charge of the micelles (Figure 12).

(iii) The cylindrical micelles have a lower degree of charging and lower electric energy per monomer, g^{el}, compared to the spherical micelles. That is the reason why the formation of cylindrical micelles is energetically favorable. When the solution was diluted the difference between the values of g^{el} for spherical and cylindrical micelles decreases (Figure 13), and consequently, the micelle size diminishes.

From a practical viewpoint, it should be noted that the long cylindrical micelles formed in the presence of Ca^{2+} and Al^{3+} exhibit a solubilization efficiency markedly larger than that of the common spherical micelles, see Figure 10 in ref 14. In other words, the same amount of surfactant solubilizes more oil when it is organized as large cylindrical (rather than small spherical) micelles. This finding could be employed in detergency. An extension of this study to solutions containing Ca^{2+} was recently carried out.[35]

Acknowledgment. This work was supported by the Colgate-Palmolive Co. and by the Bulgarian National Science Fund. The authors are indebted to Mr. J. Petkov for his help in the light scattering experiments, as well as to Professors A. Ben-Shaul and D. Blankschtein for the stimulating discussion of the results. The authors are grateful to Reviewers 2 and 3 for their detailed and comprehensive comments, which led to an improvement of the quality of the manuscript.

Appendix 1: Procedure of Calculation of $\bar{n}_M$, a_s and a_c

We utilized the procedure from ref 14 to calculate the micelle aggregation number, $\bar{n}_M$, using the radius and the length of the sphero-cylinders (Figure 1) determined from the dynamic light scattering data (see section 2.2). The procedure itself is the following:

(i) From the measured autocorrelation function of the scattered intensity one calculates the mass average diffusion coefficient, D, using exponential sampling method.

(ii) For the smallest *spherical* micelles from the value of D, one calculates the outer (hydrodynamic) radius of the micelle, $R_{out} = R_H$; the value of R_{out} thus obtained coincides (in the framework of the experimental accuracy) with the value $R_{out} = 2.77$ nm determined from the literature data[1,28] for the lengths of the constitutive fragments of a SDP2S molecule. The radius of the cross section of a *rodlike* micelle is assumed to be equal to R_{out}.

(iii) From the value of D for the rodlike micelles, one calculates their average length, L_H, by using eqs 2.8−2.14 in ref 14; L_H includes the length of the cylinder and the two hemispherical caps, see Figure 1.

(iv) The average volume of the hydrophobic core of a micelle, V_{core}, is then calculated from the values of L_H and R_{out} by using the following geometrical relationship

$$V_{core} = \pi(R_{out} - l_{head})^2(L_H - 2R_{out}) + {}^4/_3\pi(R_{out} - l_{head})^3 \quad \text{(A.1)}$$

Here, $l_{head} = 1.1$ nm is the length of the hydrophilic headgroup of a SDP2S molecule (2 oxyethylene groups + 1 SO_4^- group) determined from literature data.[1,28]

(v) Finally, we calculate the average aggregation number

$$\bar{n}_M = V_{core}/V_{tail} \quad \text{(A.2)}$$

where V_{tail} is the volume occupied by the hydrocarbon tail

of a single surfactant molecule; for a dodecyl chain, the literature data[1,28] yield $V_{tail} = 0.3502$ nm^3.

The values of areas per headgroup at the surfaces of the spherical and cylindrical micelles, a_s and a_c, used in the calculation procedure described in Appendix 2, are determined as follows:

(a) From the light scattering data we know that $n_0 \approx 56$; in addition, the calculations based on the light scattering data and the molecular structure yield $R = 2.57$ nm for the radius of the sphere at which the centers of the SO_4^- groups are located. Then, one obtains the area per SO_4^- group at the surface of a *spherical* micelle to be

$$a_s = \frac{4\pi R^2}{n_0} = 1.48 \text{ nm}^2 \qquad \text{(A.3)}$$

(b) Next, we calculate the area per SDP2S molecule at the sphere, which divides the hydrophobic core of a *spherical* micelle from its hydrophilic headgroup region

$$a_s^{(\text{core})} = \frac{4\pi R_{\text{core}}^2}{n_0} = 0.63 \text{ nm}^2 \qquad \text{(A.4)}$$

where $R_{core} = 1.67$ nm is the radius of the micelle hydrophobic core; $R_{core} = 1.67$ nm is also the length of a dodecyl chain.

(c) Then we use the "packing constraint" of Israelachvili et al.[15] to calculate the area per surfactant molecule at the dividing surface between the hydrophobic core and the hydrophilic headgroup region of a *cylindrical* micelle

$$a_c^{(\text{core})} \approx a_s^{(\text{core})}/1.5 = 0.42 \text{ nm}^2 \qquad \text{(A.5)}$$

(d) Finally, we estimate the area per SO_4^- group at the surface of a *cylindrical* micelle using the following geometrical relationship

$$a_c = a_c^{(\text{core})}\frac{R}{R_{\text{core}}} = 0.64 \text{ nm}^2 \qquad \text{(A.6)}$$

Note that $a_s/a_c = 2.3$, but nevertheless, the packing constraint, eq A.5, is satisfied.

Appendix 2: Numerical Procedure for Fitting the Experimental Data

The aim of the numerical procedure is to fit the experimental data from Figure 3 plotted as $\bar{n}_M$ vs $t \equiv [K_{dl}(X - X_1)]^{1/2}$, see eq 4.1. $\bar{n}_M$ is given by the experiment. In addition, we have $X - X_1 = 0.018(c_s - \text{cmc}) = 0.018c_{SM}$ where the values of c_s and cmc (in mol/L) are also known from the experiment. Therefore, the main efforts are directed to the calculation of K_{dl} for given values of c_{SM} and ξ.

1. The input parameters are $R = 2.57 \times 10^{-7}$ cm, $e = 4.8 \times 10^{-10}$ CGSE units, $kT = 4.1 \times 10^{-14}$ erg, $\epsilon = 77.5$, $\epsilon_{st} = 55.5$; the diameters of Na^+ and Al^{3+} ions are $\delta_N = 0.72$ nm and $\delta_A = 0.96$ nm, respectively; the aggregation number of the smallest spherical micelles is $n_0 = 56$. The values of ξ for the separate experimental curves are shown in Figure 3; c_{SM} is an input variable characterizing the experimental points, see also eq 3.5. The constant in the Langmuir isotherm, eq 2.13, is also known: $B = 8.5 \times 10^{-5}$ M.

In the case of *cylindrical* micelle we set

$$m = 1, \quad a = 0.64 \text{ nm}^2 \qquad \text{(B.1)}$$

In the case of *spherical* micelle we set

$$m = 2, \quad a = 1.48 \text{ nm}^2 \qquad \text{(B.2)}$$

(see Appendix 1 for the values of a). The adjustable parameters are K_{ndl} and the thickness of the Stern layer, δ, see eqs 3.6 and 3.27. From the input value of δ, we calculate Φ_A and Φ_N from eqs 3.27 and 3.28.

2. For given c_{SM} and ξ, we calculate c_{AB} from eqs 2.12 and 2.13. Then, I_t is calculated from eq 3.4, and c_{NB} is calculated from the equation

$$c_{NB} = 2I_t - I_0 - 9c_{AB} + 3c_{AT} - \text{cmc} \qquad \text{(B.3)}$$

which follows from eqs 3.3 and 3.4; $I_0 = 0.024$ M and $a_{Na} \approx 0.20$; the results are not sensitive to the value of α_{Na}. Then we calculate κ and λ from eq 3.13.

3. Further, assuming a tentative value of y_0, we calculate u, $J(u)$, s, b_N, and b_A from eqs 3.19−3.21 and 3.26. Then, $\alpha(y_0)$ is calculated from eqs 3.24 and 3.25. The results are substituted in the equation

$$\alpha^2\left(\frac{4\pi e^2}{\epsilon kTa\kappa}\right)^2 = 4\sinh^2\frac{y_0}{2} + \lambda^2 u^6(1 + 3e^{-y_0}) + \frac{2m}{\kappa R}\left[8\sinh^2\frac{y_0}{4} + \lambda J(u)\right] \qquad \text{(B.4)}$$

(stemming from eqs 3.14, 3.21, and 3.23), which is solved numerically to determine y_0. In this way, one obtains also the values of θ_A, θ_N, and α.

4. Next, we calculate g^{el} by means of eq 3.22, where σ and s are given by eqs 3.21 and 3.23. The integral in 3.22 is to be solved by numerical integration.

5. The values of g^{el} calculated for cylinder, eq B.1, and for sphere, eq B.2, are substituted in eq 3.7, and thus, K_{dl} is determined.

6. For each experimental value of $X - X_1$, we calculate the quantity $t \equiv [K_{dl}(X - X_1)]^{1/2}$. The theoretical value of $\bar{n}_M$ is calculated by means of eq 4.1.

7. The adjustable parameters δ and K_{ndl} are determined from the fit of the experimental data for $\bar{n}_M$ vs t by means of the least-squares method by minimization of the function $\psi(\delta, K_{ndl})$ in eq 4.2. For $\xi = 0.67$ we obtain $K_{ndl} = 1.08 \times 10^7$. Since K_{ndl} is not expected to depend on ξ, we fixed $K_{ndl} = 1.08 \times 10^7$ and processed the data for the other values of ξ ($0.73 \le \xi \le 1.23$, see Figure 3) with a single adjustable parameter, δ.

LA970684X